

# Petrographical and Petrophysical Studies of Some Upper Cretaceous Rocks, Western Desert, Egypt

Hesham Abuseda<sup>1</sup> and Abdel Muktader El\_Sayed<sup>2</sup>

<sup>1</sup>Production Department, Egyptian Petroleum Research Institute (EPRI), 11727, Cairo, Egypt.

<sup>2</sup>Department of Geophysics, Faculty of Sciences, Ain Shams University, 11566 Cairo, Egypt.

Received 20 June 2021; Accepted 27 July 2021

## Abstract

The petro-graphically studied sandstone samples are principally made out of detrital quartz and quartz overgrowth, plagioclase, microcline, kaolinite, iron oxide, and pyrite. Muscovite, biotite, apatite, and calcite, are present as accessory minerals. The sedimentary structures show that the deposition environment was in a relatively low-energy, sub- to the intertidal zone. The petrophysical properties indicate a moderate degree of diagenesis and cementation for the investigated sandstones that results in favorable reservoir conditions. Most samples belonging to the Bahariya Formation showed a strong influence on most petrophysical parameters. It causes a higher internal surface ( $S_{por}$ ), higher electrical resistivity, higher magnetic susceptibility, increased p-wave velocity, a small reduction in porosity, and reduced rock permeability. Magnetic susceptibility has proved to be a key parameter in evaluating the investigated sandstone samples' porosity and permeability. Iron oxide cement that has been precipitated in the pore space control porosity, specific internal surface, and permeability. The permeability–formation resistivity factor relation reflects the effect of porosity changes, as indicated by Archie's law. The pore volume-related internal surface shows an inverse relation to permeability for both Bahariya and Abu Roash formations. Since it is known that ( $S_{por}$ ) is related to the inverse to the effective pore radius. The formation factor's determination from the Börner equation has been determined and is slightly lower than in the measured formation factor. It was shown that the Wyllie equation fails to provide a reliable prediction of porosity for saturated samples from compressional wave velocity data.

© 2022 Jordan Journal of Earth and Environmental Sciences. All rights reserved

**Keywords:** Permeability, Porosity, Susceptibility, Spectral Induced Polarization.

## 1. Introduction

The Abu Sennan concession lies in the Western Desert, Egypt, which is considered one of the most important oil and gas provinces. The Abu Sennan concession is located between latitudes 29° 32' and 29° 35' N and longitudes 28° 30' and 28° 35' E. (see Figure 1). It lies 260 km west of Cairo and about 160 km south of the Mediterranean coast. The South West Sennan (SWS) oil field is in the Abu Sennan concession. The Upper Cretaceous (Cenomanian) Bahariya Formation is counted among the most important hydrocarbon reservoirs in the Western Desert. Several authors studied the subsurface Bahariya Formation from the stratigraphic, tectonic, and sedimentological points of view (Soliman and Hassan, 1970; El Gezeery et al., 1972; Franks, 1982, Dominik, 1985; and Catuneanu et al., 2006). It is made up of sandstones, siltstones, shale, and limestone. Catuneanu et al., 2006 described the Bahariya depositional environment as an overall transgression with coastal backstepping comprising several coarsening-upward cyclothems and the deposition of fossiliferous glauconitic siltstones and sandstones. Hence, the environment was a shallow marine with tidal flat to marine

shelf settings. The stratigraphic sequence of the SWS field can be described by the generalized stratigraphic column of the northern part of the Western Desert shown in Figure 2. The Khoman, Abu Roash, and Bahariya formations form the Upper Cretaceous section in the stratigraphic column. The Bahariya is the lowermost Formation, which covers the lower Cretaceous Kharita Formation. The Abu Roash Formation overlies it that consists of limestone, shale, and sand interbeds, which were deposited under restricted marine conditions Abuseda et al., 2016. The present study is mainly devoted to the analysis of core samples recovered from four wells, SWS-7, SWS-13, SWS-15, and SWS-21, related to the Bahariya Formation, and two wells SWS-8 and SWS-21 related to Abu Roash Formation have been investigated to establish useful relations between petrophysical parameters and reservoir properties. The samples' mineralogical composition was analyzed by microscopy of thin sections and scanning electron microscope (SEM). Different petrophysical methods were applied to identify the sample's physical parameters related to reservoir properties.

\* Corresponding author e-mail: heshamabuseda@epri.sci.eg

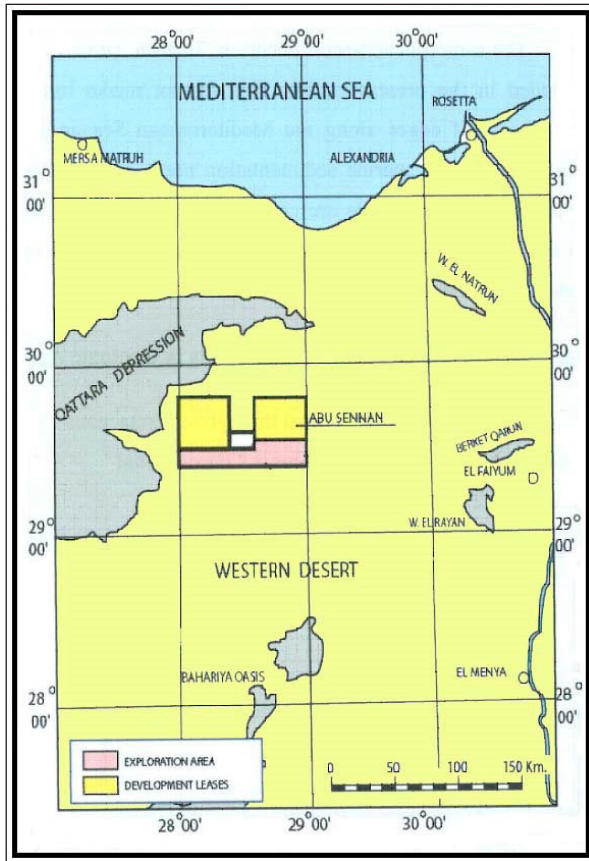


Figure 1. location map of the study area.

## 2. Mineralogical investigations

The petrography and mineralogy of the present studied samples were examined using a polarizing microscope and the description was based on the study of the petrography and facies types. The sedimentary structures and mineralogical composition correspond to the results of Athmer (2006) and Halisch et al. (2009). The mineralogical composition and the sedimentary structures studied by Abuseda et al., 2016 show that the sedimentary structures show characteristic deposition features in a relatively low-energy, sub- to the intertidal zone. To identify the mineralogical composition of sandstones of the SWS field, a variety of thin sections were prepared for transmitted light microscopic investigations. These investigations reveal that the mineralogical composition for studied sandstone samples is mainly composed of detrital quartz and quartz overgrowth, kaolinite, plagioclase, and microcline, pyrite. Muscovite, biotite, zircon, glauconite, rutile, apatite, and diagenetic calcite, are present as accessory minerals. The mica minerals have a fibrous shape and are located tangential between quartz grains, which indicate deep burial Figure 3, showing a primary inter-particle porosity (yellow arrow) and the (red arrows) indicate tangential mica between quartz grains. Cementation minerals are kaolinite, calcite, and subordinate quartz overgrowths Figure 4, with associated secondary microporosity (Alsuwaidi et al., 2021). Most of the quartz overgrowth surfaces are clean of further cement forming diagenetic minerals (Farouk et al., 2018). Non-weathered tight glauconite grains, as well as disintegrating glauconite grains with secondary intraparticle microporosity, indicate moldic porosity. Feldspar appears as plagioclase and microcline, which often are heavily etched or decomposed to honeycomb structures. Muscovite is mostly aligned along with the sedimentary beddings. Due to their oxidation, the layers contain minor iron hydroxides and quartz overgrowths Figures 5 & 6. Abundant chlorite cementation increases the magnetic susceptibility, the specific internal surface, and grain density and, on the other hand, decreases porosity and permeability.

## 3. Petrophysical investigation

Petrophysics is considered a cornerstone and magic key for solving geophysical problems and introducing theories. Therefore, the study of rock physics provides multidisciplinary concepts and tools to facilitate and enhance geophysical interpretation. Laboratory investigations were carried out to determine standard parameters for reservoir characterization, such as porosity, density, permeability, and special core analysis, such as specific surface area, compressional wave velocity, and complex electrical resistivity. We combined the knowledge and data of geology, mineralogy, and petrophysics to get access to form a detailed reservoir description.

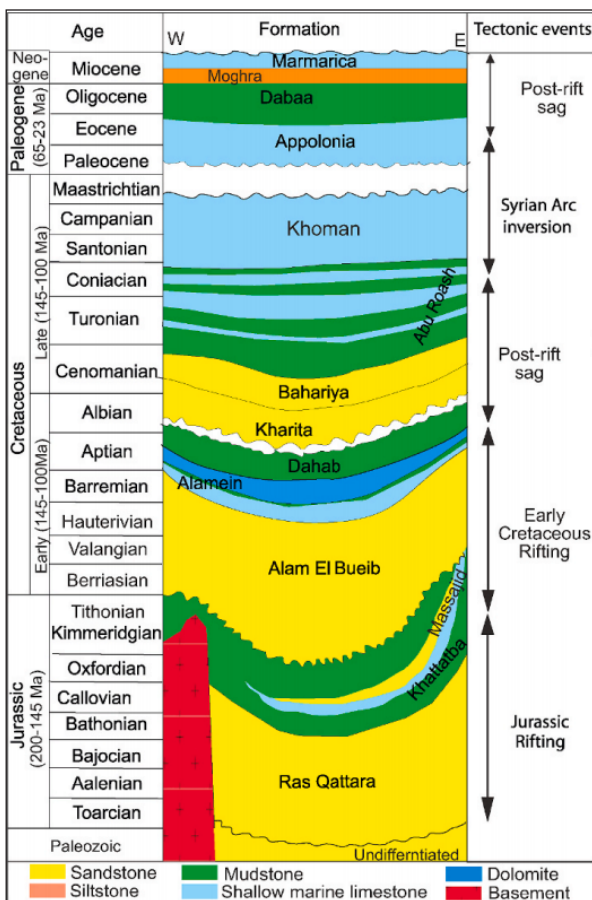
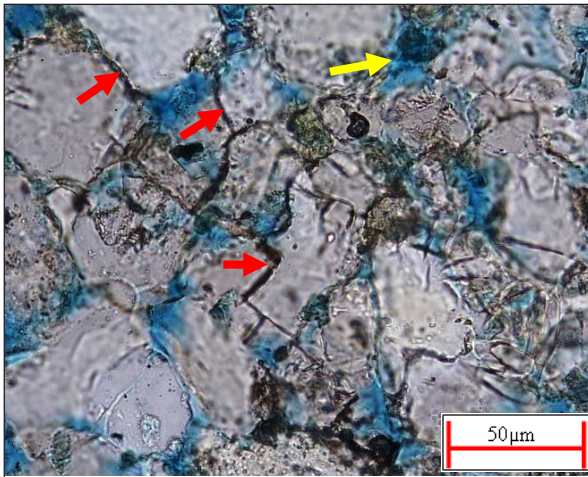
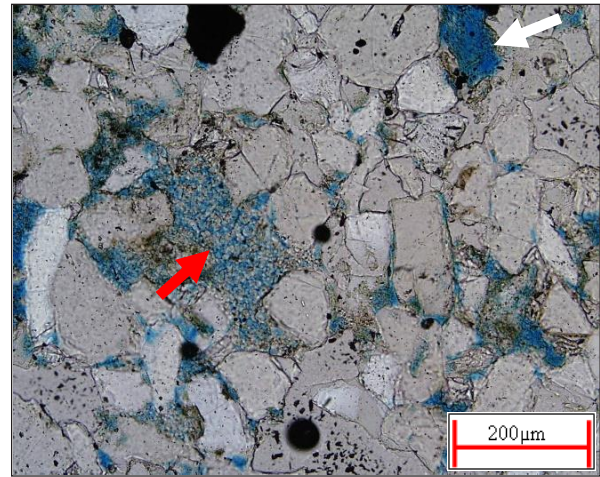


Figure 2. Stratigraphic column of the Western Desert (Selim et al., 2021).



**Figure 3.** Thin section image of sample 15\_28H1 (PPL X40) Bahariya Formation. They are showing primary interparticle porosity (yellow arrow). The red arrows indicate tangential mica between quartz grains.



**Figure 4.** Thin section image of sample 15\_43H1 (PPL X40) Bahariya Formation. They are showing pore filling kaolinite (red arrow) with associated secondary microporosity.

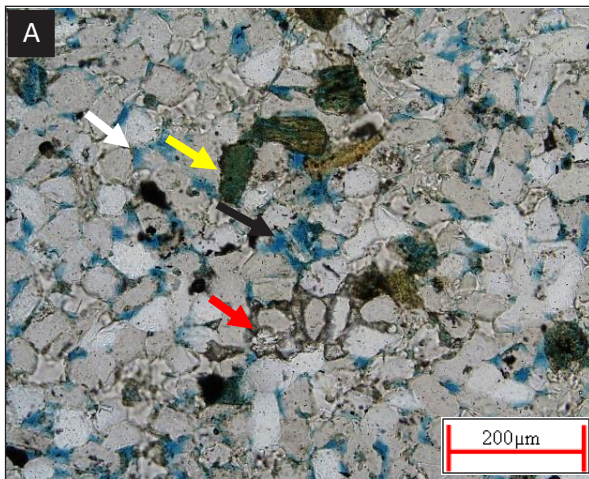


**Figure 5.** Thin section image of sample 15\_28H1 (PPL X10) Bahariya Formation. (A) Primary interparticle porosity (white arrow), secondary moldic porosity (black arrow), secondary intraparticle microporosity within a glauconite grain (yellow arrow), and carbonate cement (red arrow). (B) SEM image showing a moderate increase of specific internal surface by glauconite grains (red arrows) and feldspar honeycombs (white arrow). Pore-lining cement of Fe-rich chlorite is missing or less. Most of the quartz overgrowth surfaces (yellow arrow) are clean of further cement forming diagenetic minerals.

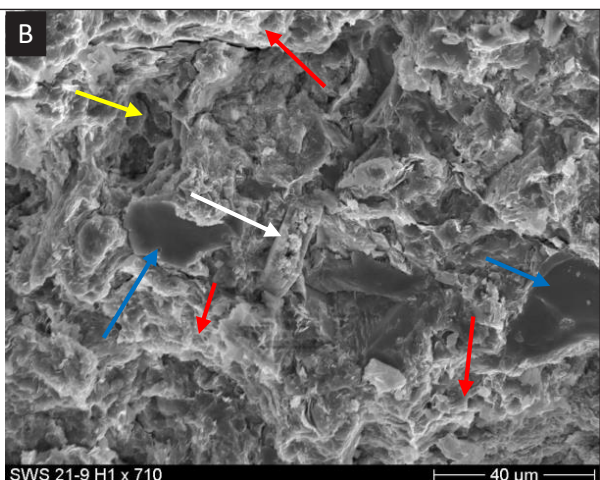
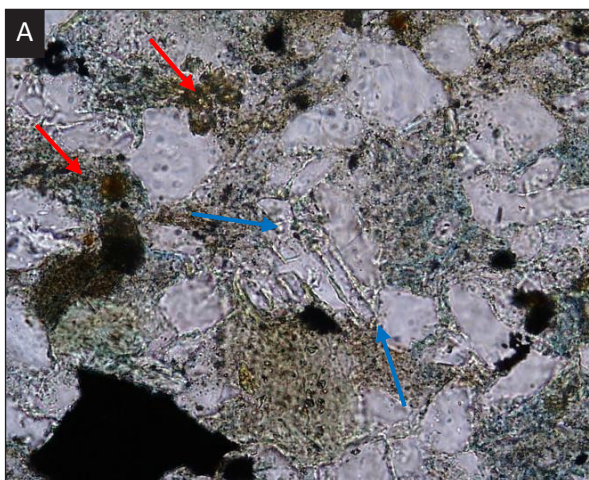


**Figure 6.** Thin section image of sample 21-9H1 (PPL X10) Abu Roash Formation. Silty quartz and quartz swimming in shale (blue arrows) stained by iron oxide (red arrows). (B) SEM image showing a strong increase of specific internal surface by pore-lining cement of Fe-oxide (red arrows) and clay matrix (white arrow). The amount of quartz overgrowth surfaces (blue arrows) cleans of further cement forming diagenetic minerals is rather low. The yellow arrow indicates a pyrite

3.1. Methods and Techniques:

- Petro-physical properties

3.1.1. Sample preparation:

Samples were drilled as cylinders of 2.5 cm diameter and different lengths (2 to 4 cm) using a diamond drilling machine. The studied samples have been cleaned by organic solvents using soxhlet extractor apparatus; the particular solvent used was selected not to alter or destroy the samples pore framework. Samples were dried to remove pore water and cleaning solvent. It dried in an oven to a constant weight of 100 C°. Before and after a subsequent 4 hours drying period, samples were at a constant weight, and repeatable weight (+/- 1%) could be determined. After constant weights had been achieved, all the samples were cooled to room temperature in moisture-free desiccators.

3.1.2. Porosity and density

Several methods have been proposed and explained in different literature for rock porosity determination. In the laboratory, measurement of rock porosity requires the determination of only two of the three-volume parameters: they are pore volume (V<sub>p</sub>), grain volume (V<sub>g</sub>), and bulk volume (V<sub>b</sub>), with the latter being the sum of the previous two parameters. In the present study, the rock porosity and grain density were determined by the Archimedes method with weighting the sample three times: in a dry state, in a fully saturated state, and finally in a water basin. Bulk density is defined as the mass of the unit volume of a rock in its natural state and expressed as:

$$d_b = \frac{m}{V} \dots\dots\dots (1)$$

with bulk density g/cm<sup>3</sup>, mass of the sample g, and volume of the samples cm<sup>3</sup>.

The grain density is a sensitive tool to indicate the mineral composition of the rock. It also helps in the evaluation of the cement materials and the presence of impurities. It has been calculated from the porosity test (Archimedes method) by using the following equation:

$$d_g = \frac{m_d}{V_g} \dots\dots\dots (2)$$

with grain density g/cm<sup>3</sup>, dry mass of sample g, and volume of grains cm<sup>3</sup>.

Porosity is the most important parameter for evaluating the storage capacity of a porous medium. Porosity (Φ) is defined as the ratio of the volume of pore space V<sub>p</sub> to the total volume V of the rock sample:

$$\Phi = \frac{V_p}{V} \dots\dots\dots (3)$$

with volume of pore space cm<sup>3</sup>, volume of the samples cm<sup>3</sup>, and porosity.

3.1.3. Specific surface area

Porosity describes the volume of the voids (pores, cracks, fissures, fractures, etc.) related to the considered rock volume. The specific internal surface describes the surface area of these voids to S<sub>tot</sub>. (μm<sup>-1</sup> the total rock volume) with S<sub>por</sub> μm<sup>-1</sup> (the pore volume) with S<sub>m</sub> μm<sup>-1</sup> (the volume of the solid matrix) and S<sub>ma</sub> m<sup>2</sup>/g (the mass of the dry rock). The following equations can be used to transform the quantities

mentioned above:

$$S_{por} = d_{grain} \left( \frac{(1 - \Phi)}{\Phi} \right) S_m$$

$$S_{tot} = \Phi \cdot S_{por} = (1 - \Phi) \cdot S_m \dots\dots\dots (4)$$

$$S_{ma} = \frac{S_m}{d_m} \dots\dots\dots (5)$$

with density of the solid matrix material.

The specific internal surface depends mainly on the shape and size of pores and the matrix-pore interface's microstructure and morphology. The specific internal surface varies over a wide range. The "micromorphology" of the pore surface strongly influences the value of the specific internal surface. The specific internal surface increases with the decrease of the mean pore or grain size as a general tendency. The presence of clay particles and the growth of various types of surface structures in the pore space increases the internal surface (Schön, 1996).

3.1.4. Permeability

The permeability of a rock is defined as a measure of a porous material's ability to transmit fluid. Permeability is a phenomenon that can be described by Darcy's law for viscous fluids in porous media. A rock's permeability is controlled by many factors such as rock pore geometry, cementation, rock texture, grain size, grain shape, and roundness.

Molecular slip can contribute to the flow of gases when the pore dimensions approach the gas molecules' mean free path. The apparent permeability k<sub>a</sub> becomes dependent on the mean absolute gas pressure (Klinkenberg, 1941)

$$k_a = k \left( 1 - \frac{a}{p} \right) \dots\dots\dots (6)$$

The constant called Klinkenberg constant. The Klinkenberg constant is often expressed as a function of the true permeability k. The Klinkenberg effect might even lead to a "gas chromatographic" separation of gases of different molecular weights in porous rocks. In geohydrology, a simplified version of Darcy's law is commonly used.

3.1.5. Magnetic Susceptibility

The magnetic properties of rocks are controlled by those mineral constituents which have a magnetic effect. The fraction of these minerals concerning the total rock volume may be small. Magnetic properties describe the behavior of any substance under the influence of a magnetic field. Magnetic phenomena arise from the motion of electrically charged particles within the substance. Schön (1996) describes three main groups of materials about the magnetic properties: diamagnetic behavior, Paramagnetic behavior, and Ferro-, antiferromagnetic and ferrimagnetic behavior. Diamagnetic and paramagnetic substances show only weak effects in the presence of an applied magnetic field. In both cases, the strength of the induced magnetization M (magnetic dipole moment per unit volume) is directly related to the strength of the applied magnetic field H:

$$M = \kappa \cdot H \dots\dots\dots (7)$$

with the factor of proportionality κ being the magnetic susceptibility.

### 3.1.6. Formation Resistivity Factor

The formation resistivity factor was discussed by many authors, such as Wyllie and Spangler, 1952; El Sayed, 1981; Tiab and Donaldson, 2015; Glover, 2009; Abuseda et al., 2016 and others. They concluded that the formation resistivity factor is a function of the effective electric current flow path and the effective cross-sectional area available for electric conduction.

Archie (1942) first defined the property of a porous medium known as “formation resistivity factor” as:

$$\text{True formation resistivity} = \frac{R_w}{rho_0} \dots\dots\dots (8)$$

with the photo being the resistivity of a sample that is completely saturated with brine of resistivity  $R_w$ .

The fundamental formation resistivity factor F porosity relation, as introduced by Archie (1942), is

$$F = \Phi^{-m} \dots\dots\dots (9)$$

with m being the cementation factor.

Wyllie and Gregory (1953) investigated the influence of particle size and cementation on the formation resistivity factor of various materials. Observed formation resistivity factor for artificially cemented aggregates showed that the cemented aggregates exhibit a greater change in porosity than the unconsolidated aggregates. Wyllie and Gregory (1953) concluded that the general form of the relation between formation factor and porosity is:

$$F = a\Phi^{-m} \dots\dots\dots (10)$$

with a being another free parameter that depends on lithology.

At high water salinity, the measured ratio is a good estimate of the true formation factor.

### 3.1.7. Compressional wave velocity

The elastic properties and the velocity of elastic waves in

rocks are controlled primarily by the rock-forming minerals and constituents’ elastic properties, their fractional volume, their contact, cementation or bonding properties, pressure, and temperature. The mineralogical composition of sedimentary rock has a strong influence on its velocity. For certain rock types, porosity is often the dominant influence. The elastic properties of porous clastic and carbonate rocks are mainly controlled by porosity and matrix composition. The matrix composition also influences the contact conditions, cementation, and grain bonding (Schön, 1996). In the present work, compressional wave velocity was measured at room temperature and ambient pressure on cylindrical samples using USLT 2000 (Inspection Technology). The acoustic velocity was determined for fully saturated sandstone rock samples at ultrasonic frequencies of 500 kHz. Porosity is one of the most important characteristic parameters in the evaluation of potential reservoirs. The porosity can be derived from the knowledge of the interval velocity. The average time equation of Wyllie et al., (1956 and 1958) has been used to obtain porosity from acoustic velocity logs. The equation for P-wave velocity ( $V_p$ ) in water-saturated rock is:

$$\frac{1}{V_p} = \frac{\Phi}{V_f} + \frac{(1-\Phi)}{V_m} \dots\dots\dots (11)$$

$$\Phi = \frac{V_f (V_m - V_p)}{V_m - V_f} \dots\dots\dots (12)$$

with:  $V_p$  the compressional wave velocity,  $V_m$  the velocity of the solid material,  $V_f$  the velocity of the pore fluid, and  $\Phi$  the porosity of samples.

This simple equation appears adequate for fully saturated sandstone in the middle range of porosity ( $10\% < \Phi < 25\%$ ).

## 4. Results and Discussions

The minima, maxima, average values, and standard deviations of all measured parameters are calculated for all studied samples are compiled in Table (1).

**Table 1.** Compilation of minimum, maximum, average values, and standard deviations of measured petrophysical parameters.

Parameters	Bahariya Formation				Abu Roash Formation			
	Min.	Max.	Mean	Std. dev.	Min.	Max.	Mean	Std. dev.
<i>dry</i> (g/cm <sup>3</sup> )	2.00	2.42	2.17	0.14	1.94	2.59	2.18	0.18
<i>drain</i> (g/cm <sup>3</sup> )	2.52	2.84	2.65	0.08	2.24	2.73	2.57	0.15
Porosity $\Phi$	0.12	0.24	0.18	0.04	0.05	0.26	0.15	0.07
Permeability (MD)	0.06	133.65	44.35	51.28	0.05	25.36	11.27	12.11
F	12.45	62.40	26.23	13.22	13.27	38.01	22.66	13.40
$\kappa$ (10 <sup>-6</sup> SI)	25.19	1175.05	235.18	253.96	7.33	906.98	177.88	152.10
VP (m/s)	2053	3880	2851	435	2190	3887	2875	413
$S_{por}$ (1/ $\mu$ m)	1.35	147.91	40.33	45.94	13.01	43.79	24.92	13.67
$s'$ (mS/m)	5.64	26.39	13.20	6.76	1.93	13.43	8.98	4.93
$s''$ (mS/m)	0.04	0.32	0.15	0.08	0.02	0.26	0.17	0.11
$\sigma'_{surf}$ (mS/m)	0.99	22.77	8.06	7.35	4.27	7.60	5.95	1.66
$r$ ( $\Omega$ m)	38.75	181.86	99.06	42.87	98.90	103.85	100.69	2.19

**4.1. Bulk density - porosity relationship**

The bulk density - porosity relationship for the studied samples is shown in Figure 7. An inverse relationship for all studied Bahariya Formation wells encountered in SWS-7, SWS-13, SWS-15, SWS-21, and Abu Roash Formation in wells SWS-8, SWS-21 is characterized by a coefficient of correlation ( $R^2 = 0.78$  and  $0.76$ ) for the Bahariya Formation and the Abu Roash Formation respectively.

The following equations control the bulk density - porosity relationship Figure 7:

$$\text{For the Bahariya Formation } \Phi = 0.68 - 0.23 d_b \dots\dots\dots(13)$$

$$\text{For the Abu Roash Formation } \Phi = 0.79 - 0.29 DB \dots\dots(14)$$

with the bulk density  $d_b$  given in  $g/cm^3$  and the porosity  $\Phi$  as fraction value.

**4.2. Porosity - Permeability relationship**

The permeability of a rock may be affected by many geological factors. High rock porosity does not guarantee that a significant permeability exists. The pores must be interconnected, and the pore throats must be large enough to permit the flow of fluids. A pore network is made up of larger spaces referred to as pores, which are connected by small spaces referred to as pore throats. In other words, the volume of pore space is reflected by the measured porosity, while the measured permeability of the rock reflects the size of pore throats. The geometric relationship between pore spaces and pore throats controls the relationship between porosity and permeability. The relationship between porosity and permeability has been studied by many authors, (e.g., Carman, 1937; Timur, 1968; Scheidegger, 1974; El Sayed, 1981; Herron, 1987; Adler et al., 1990; Schön, 1996; and Tiab and Donaldson, 2015). In the present work, porosity-log permeability cross plots exhibiting the investigated samples are shown in Figure 8. This figure's data points follow the expected positive trend between porosity and permeability for all studied samples. The relationship is characterized by a weak coefficient of correlation ( $R^2 = 0.43$ ) for the Bahariya and a high correlation coefficient ( $R^2 = 0.88$ ) for the Abu Roash Formation, indicating the inhomogeneity of the Bahariya Formation. The samples generally show lower porosity and permeability for all samples indicating that clay pore filling causes a decrease in porosity and permeability. The following equations control them:

$$\text{For Bahariya Formation } \ln(k) = 61.79 \Phi - 9.69 \dots\dots(15)$$

$$\text{For Abu Roash Formation } \ln(k) = 50.38 \Phi - 9.56 \dots\dots(16)$$

with the Permeability  $K$  in  $mD$  and the porosity  $\Phi$  as fraction value.

**4.3. Internal surface ( $S_{por}$ ) - permeability relationship**

The internal surface ( $S_{por}$ ) - permeability relationship for the studied samples is shown in the Figure 9. The Bahariya Formation relationship is characterized by a coefficient of

correlation ( $R^2 = 0.70$ ) and a weak coefficient of correlation ( $R^2 = 0.28$ ) for the Abu Roash Formation. The internal surface ( $S_{por}$ ) - permeability relation shows a reverse trend with a general permeability decreases with increasing internal surface ( $S_{por}$ ). Generally, the internal surface ( $S_{por}$ ) decreases with increased permeability. The following power-law equation controls the relationship:

$$\text{For Bahariya Formation } \ln(K) = 5.90 - 1.57 \ln(S_{por}) \dots(17)$$

with  $S_{por}$  Internal surface in  $10^6 * 1/m$ .

**4.4. Porosity - Formation resistivity factor relationship**

The porosity-formation resistivity factor cross plot for the studied samples is shown Figure 10. The data shows a reverse trend for all samples. The relations are characterized by the coefficient of correlation ( $R^2 = 0.70$ ) for the Bahariya Formation, but it was ( $R^2 = 0.99$ ) for the Abu Roash Formation. It shows a good possibility to calculate the formation factor from porosity data. Larger values of the formation factor reflected the samples' lower porosity, while the calculated cementation factor for the Bahariya Formation ( $m=2.05$ ) was higher than the cementation factor for the Abu Roash Formation ( $m=1.83$ ). The iron oxide improves the cementation exponent of the Bahariya sandstone due to its high electrical conductivity. The formation resistivity factor - porosity relationships are controlled by the following equations:

$$\text{For Bahariya Formation } \log F = 3.96 - 2.05 \log \Phi \dots(18)$$

$$\text{For Abu Roash Formation } \log F = 3.75 - 1.83 \log \Phi \dots(19)$$

The above equations (18 & 19) are very important for outlining these formations' water and hydrocarbon saturation during well logging processing and interpretation.

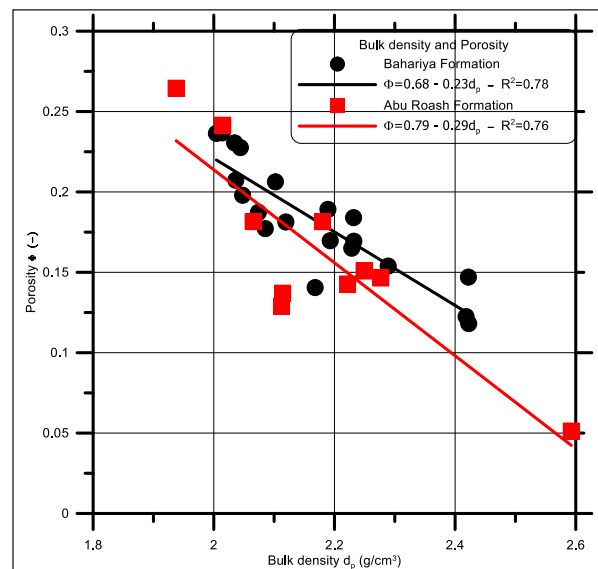


**Figure 7.** Bulk density versus Porosity for the studied samples.

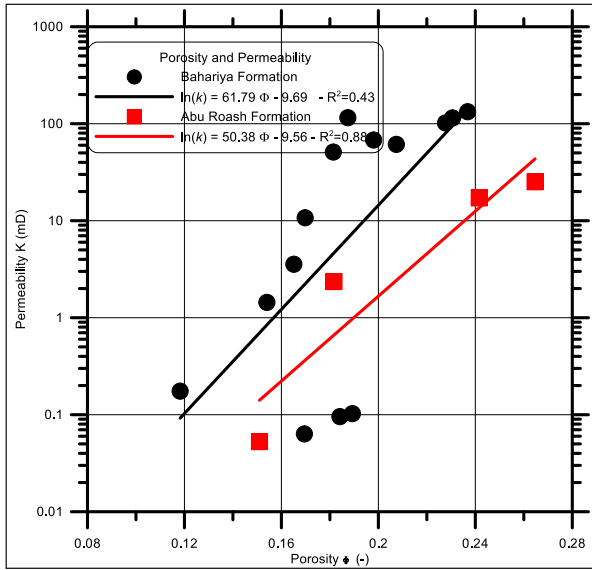


Figure 8. Porosity versus Permeability for the studied samples.

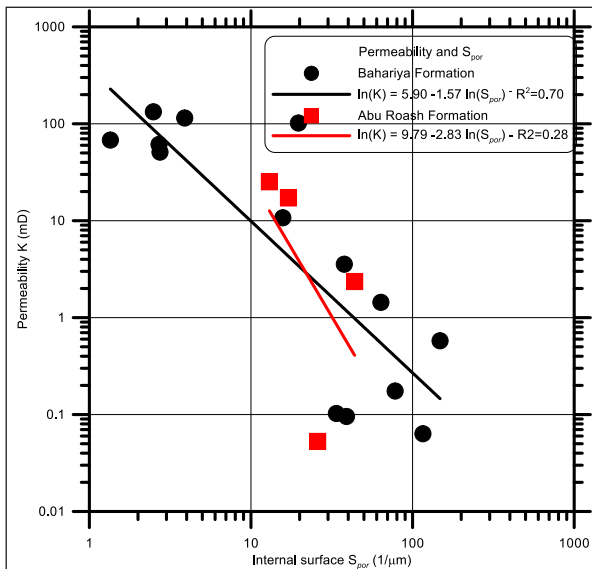


Figure 9. Internal surface  $S_{por}$  versus permeability for the studied samples.

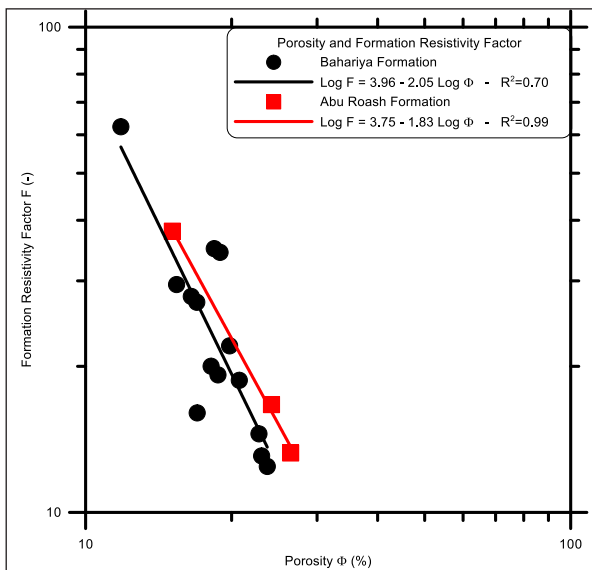


Figure 10. Porosity versus Formation resistivity factor for the studied samples.

4.5. Permeability - Formation resistivity factor relationship

The formation resistivity factor - permeability cross plot for the studied samples is shown in Figure 11. The data in this Figure show a reverse relation for all samples. The relations are characterized by a coefficient of determination of 0.69 for the Bahariya Formation, but the determination coefficient is 0.98 for Abu Roash Formation. The formation resistivity factor - permeability relationships are controlled by the following equations:

For Bahariya Formation  $\ln(K) = 19 - 5.46 \ln(F) \dots\dots(20)$

For Abu Roash Formation  $\ln(K) = 19.66 - 6.18 \ln(F) \dots(21)$

4.6. Magnetic susceptibility - Grain density relationship

The susceptibility - grain density cross plot for all samples is shown in Figure 12. The relationship is characterized by the coefficient of correlation ( $R^2 = 0.66$ ) for Bahariya Formation and is characterized by a coefficient of determination of 0.61 for Abu Roash Formation. Figure 12 indicates a positive trend of increasing magnetic susceptibility with increasing grain density for all samples. The susceptibility - grain density relationship is controlled by the following equations:

For Bahariya Formation  $\ln(d_g) = 0.02 \ln(\kappa) + 0.86 \dots(22)$

For Abu Roash Formation  $\ln(d_g) = 0.03 \ln(\kappa) + 0.80 \dots(23)$

with  $d_g$  grain density in  $g/cm^3$  and  $\kappa$  magnetic susceptibility in  $10^{-6}$  SI.

The magnetic susceptibility is a reliable indicator of the presence of iron oxide minerals. The reason for the wide variation in grain density has been identified as the increase in grain density caused by iron oxide cement, as indicated in the Figures 5 and 6.

4.7. Magnetic susceptibility and porosity relationship

The susceptibility - porosity cross plot for the samples is shown in Figure13 (the resulting correlation is characterized by a coefficient of determination of 0.51 for the Bahariya Formation and a very weak coefficient of determination for the Abu Roash Formation. The relation indicates a decreasing porosity with increasing magnetic susceptibility. The best-fitting equation reads:

For Bahariya Formation  $\ln(\Phi) = -0.14 \ln(\kappa) - 1.07 \dots(24)$

The reduction in porosity of samples suggests that diagenetic iron oxide precipitated as pore-lining cement, as can be observed in Figure 6.

4.8. Magnetic susceptibility - Permeability relationship

The susceptibility - permeability cross plot for the samples is shown in Figure 14. The resulting correlation is characterized by a coefficient of determination 0.77 and 0.84 for Bahariya and Abu Roash Formation, respectively. The susceptibility - permeability relationship shows a general increase of permeability with decreasing magnetic susceptibility for all samples, which is controlled by the equations:

For Bahariya Formation  $\ln(K) = 13.96 - 2.62 \ln(\kappa) \dots(25)$

For Abu Roash Formation  $\ln(K) = 46.60 - 9.19 \ln(\kappa) \dots(26)$

with K Permeability in mD.

The precipitation of pore-lining iron oxide in the pore space affects the permeability, too. Considerable reduction of permeability is observed for the samples of higher magnetic susceptibility.

**4.9. Magnetic susceptibility - Specific Internal surface ( $S_{por}$ ) relationship**

The relation between magnetic susceptibility and specific internal surface  $S_{por}$  is displayed in Figure 15. A clear trend is observed. The Figure indicates a positive trend in increasing magnetic susceptibility with the larger values of the specific internal surface for all samples. The power-law can describe the trend:

For Bahariya Formation  $\ln(S_{por}) = 1.48 \ln(\kappa) - 4.22 \dots(27)$

For Abu Roash Formation  $\ln(S_{por}) = 1 \ln(\kappa) - 2.07 \dots(28)$

The relationship between susceptibility and the specific internal surface is characterized by a coefficient of determination of 0.82 for Bahariya sandstone samples and a coefficient of determination of 0.99 for Abu Roash Formation.

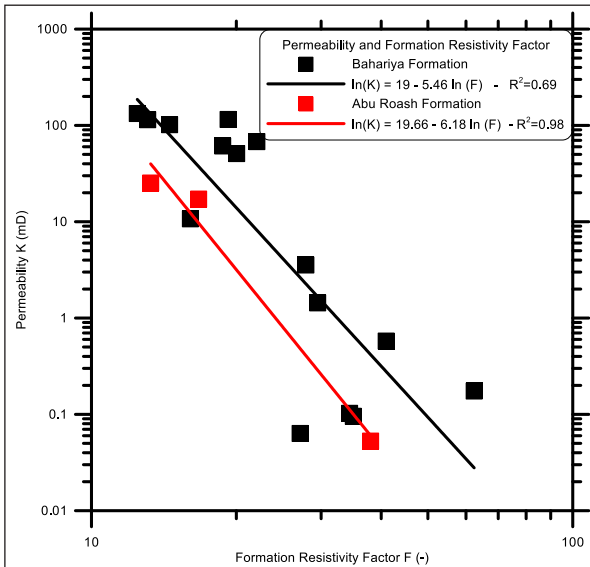


Figure 11. Permeability versus Formation resistivity factor for the studied samples.

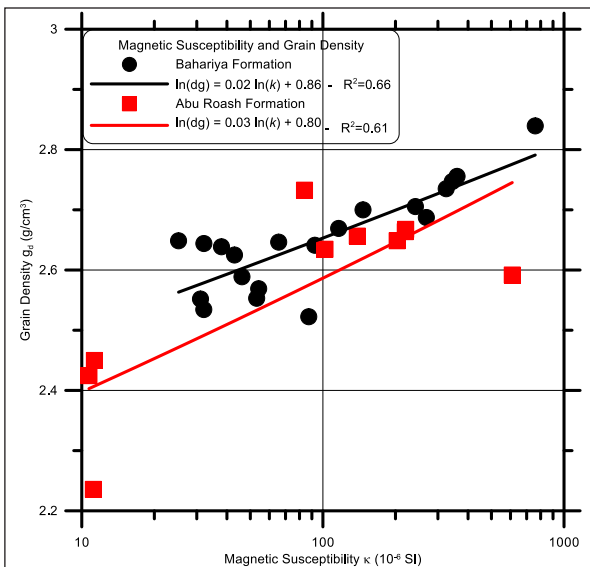


Figure 12. Magnetic susceptibility versus Grain density for the studied samples.

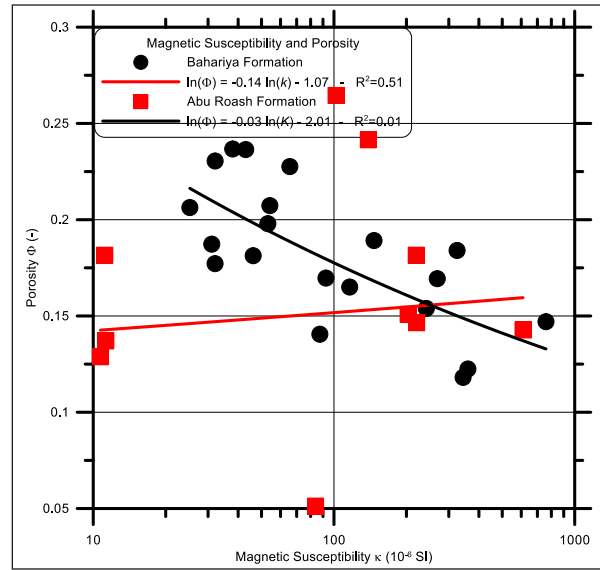


Figure 13. Magnetic susceptibility versus Porosity for the studied samples.

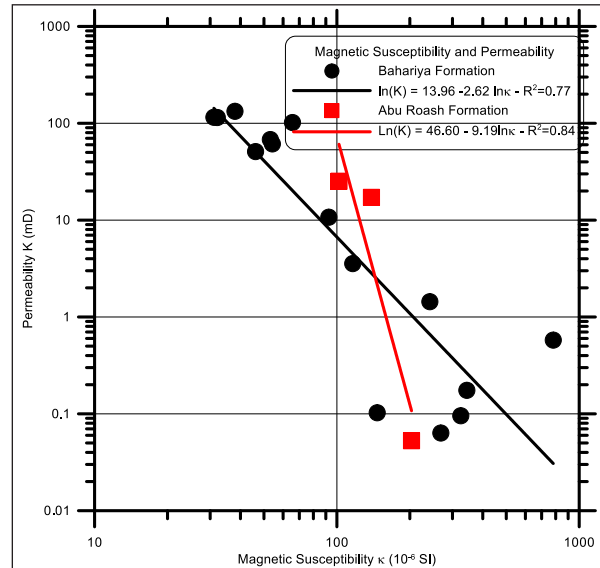


Figure 14. Magnetic susceptibility versus permeability for the studied samples.

**4.10 P-wave velocity - porosity relationship**

The p-wave velocity - porosity relationship for samples is shown in Figure 16. The relationship is characterized by a coefficient of correlation ( $R^2 = 0.49$ ). For Bahariya Formation, but the coefficient of correlation ( $R^2 = 0.77$ ) for Abu Roash Formation. The p-wave velocity - porosity shows a reverse relation. P-wave velocity decreases with increasing porosity. The following equation controls the relationship:

For the Bahariya Formation  $\Phi = 0.35 - 5.73 V_p \dots(29)$

For the Abu Roash Formation  $\Phi = 0.54 - 0.0001 V_p \dots(30)$

with:  $V_p$  compressional wave velocity.

**5. Petrophysical Models**

**5.1. Electrical parameters versus formation resistivity factor**

Most models for the complex electrical conductivity of a porous material at low frequencies (e.g., less than 100 Hz) are based on a parallel addition of two conduction terms representing (a) an electric contribution via conduction through the interconnected pore space and (b) a mineral surface conduction contribution (Vinegar and Waxman, 1984). Polarization is associated with surface conductivity at low frequencies. For a fully saturated medium:

$$\sigma_0 = \sigma_w \cdot \frac{1}{F} + \sigma_i \dots\dots\dots (31)$$

with F formation resistivity factor and  $\sigma_w$  fluid conductivity.

Empirical and mechanistic formations for the surface conductivity exist but are not established as Archie’s law. These formulations describe the surface conductivity in terms of (a) the volume normalized surface area or the cation exchange capacity and (b) factors such as the surface charge density and surface charge mobility (Waxman and Smits, 1968; Rink and Schopper, 1974; Vinegar and Waxman, 1984). Complex conductivity measurements can determine the imaginary part. Assuming a fixed ratio l between the imaginary part and real part of interface conductivity. Börner et al. (1996) report a variation of l between 0.01 and 0.15, and the true resistivity factor can be easily approximated using the following formula:

$$F = \frac{\sigma_w}{\sigma_0 - \sigma_i / l} \dots\dots\dots (32)$$

In this study, the resistivity amplitudes at a frequency of 1.0 Hz have been used. The measurements were performed under ambient conditions at a constant temperature of about 20 °C. The samples were fully saturated with a sodium chloride solution of 0.526 g/l resulting in a water conductivity of 0.1 S/m. Surface conductivity ( $\sigma'_{surf}$ ), and imaginary part of conductivity cross plot for all samples for  $\sigma_w$  100 mS/m. The data are explained by a single linear relationship with the gradient l = 0.032 for Bahariya Formation and gradient l = 0.038 For Abu Roash Formation. The equivalent relationship between surface conductivity ( $\sigma'_{surf}$ ) and normalized chargeability  $m_n$  linear relation is again observed. The gradient is equal to  $l_{mn} = 0.22$  for Bahariya Formation and gradient l = 0.23 For Abu Roash Formation. The higher value for the gradient in normalized chargeability is expected as  $m_n$  represents the total additive polarization across the measured frequency range.

Knowing the value of l provides opportunities to improve the petrophysical interpretation of electrical measurements. The inherent ambiguity of resistivity measurements results from the dependence of the measurement on the pore fluids’ properties, interconnected pore volumes, and interconnected posurfacesace. It is common practice to estimate F from measurements of  $\sigma'$  and  $\sigma_w$  at a single salinity under the assumption that the fluid’s salinity is sufficiently high such that  $\sigma_{surf}$  is negligible. Given an IP measurement, assuming l is known. According to Börner et al. (1996), a predicted value of the form factor can be determined. Figure 17 shows the result obtained using equation 33 and assuming a single value of l = 0.032 for Bahariya Formation and l = 0.038 for Abu Roash Formation. Estimated data result and relationship between surface conductivity ( $\sigma'_{surf}$ ) and an imaginary part of

conductivity cross plot. It should be noted that the variation of the formation resistivity factor calculated from the Börner formula is slightly lower than in the measured formation resistivity factor.

**5.2 Model of Wyllie equation**

The porosity can be derived from the knowledge of the interval velocity. The average time equation of (Wyllie et al., 1956 and 1958) has been used to obtain porosity from acoustic velocity logs. This simple equation appears adequate for clean sandstone in the middle range of porosity (10% <  $\Phi$  < 25%). The equations 11 and 12 for p-wave velocity in water-saturated rock. Using equation (12) to determine the acoustic porosities of the sandstone samples. The velocity of quartz = 6040 m/s is used as the velocity of the solid material VM. For the fully saturated samples, the pore space is filled with tap water, and the fluid velocity is assumed to be equal to the velocity of freshwater Vf = 1500 m/s. The comparison between the measured porosity and the acoustic porosity calculated from the Wyllie equation is shown in Figure 18. It should be noted that the variation of the acoustic porosity is larger than in the measured porosity. A strong overestimation of the acoustic porosity is observed for all samples.

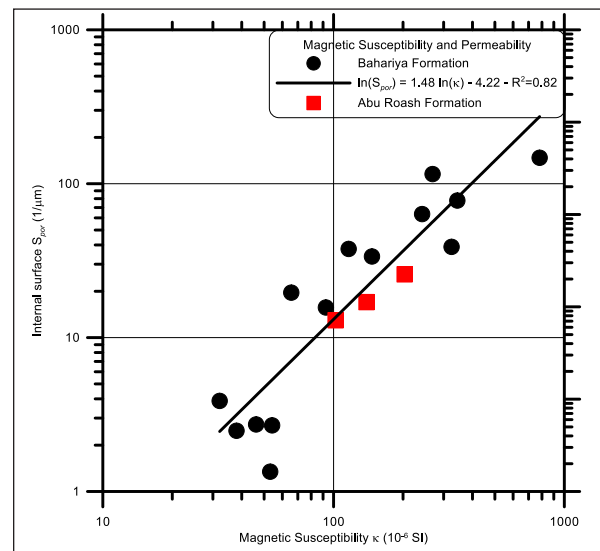


Figure 15. Magnetic susceptibility versus specific internal surface  $S_{por}$  for the studied samples.

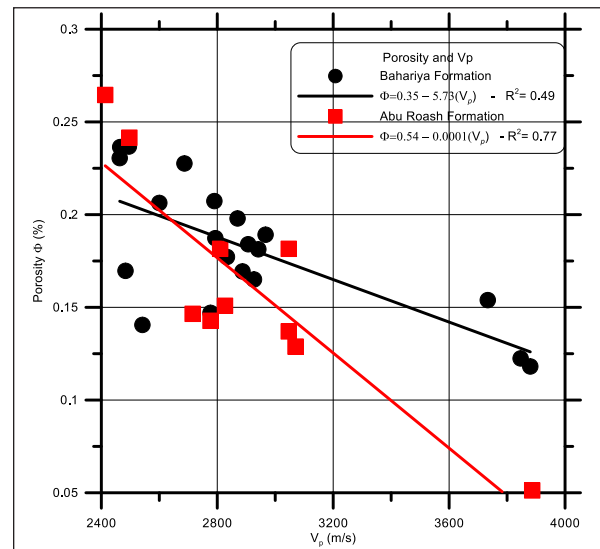
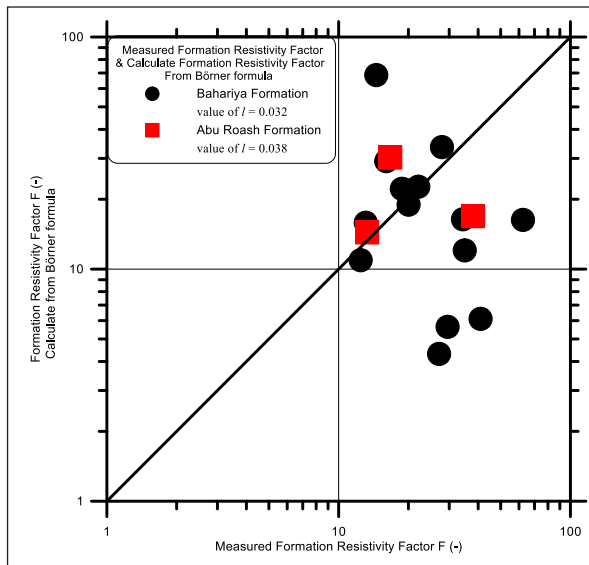
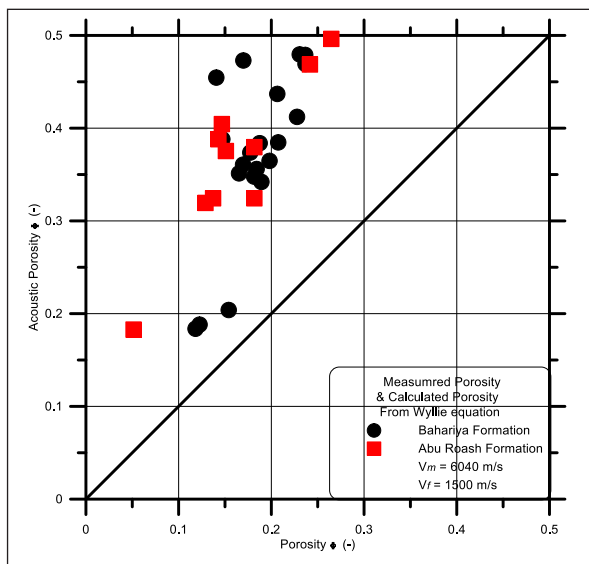


Figure 16. P-wave velocity versus porosity for the studied samples.



**Figure 17.** Measured formation resistivity factor versus calculate formation resistivity factor from Börner formula.



**Figure 18.** Measured porosity versus calculate porosity from Wyllie equation.

## 6. Conclusions

The Bahariya and Abu Roash formations represent an important Cretaceous oil and gas reservoir in Egypt. The samples of this study originate from the Abu Sennan concession in the South West Sennan oil field in the Western Desert of Egypt. The mineralogical composition for studied sandstone samples belonging to the Bahariya and Abu Rawash formations is mainly composed of detrital quartz and quartz overgrowth, kaolinite, plagioclase microcline, iron oxide, and pyrite. Muscovite, biotite, zircon, rutile, and apatite, as well as diagenetic calcite, are present as accessory minerals. The sedimentary structures show characteristic features of deposition in a relatively low-energy, sub- to the intertidal zone. Most of the samples conspicuous flaser bedding develop on tidal flats during the turn from flood to the ebb tide when transport energy reaches its lowest level so that fine material like clay and silt sinks and gets deposited between sand ripples, as demonstrated.

Most samples belonging to the Bahariya Formation were laminated and showed a strong influence on most petrophysical parameters. It causes a higher internal surface ( $S_{por}$ ), higher electrical resistivity, higher magnetic susceptibility, increased p-wave velocity, a small reduction in porosity, and reduced rock permeability. The wide variation in grain density has been identified as the increase in grain density that is caused by iron oxide cement.

The correlations of different parameters with permeability are of great interest for reservoir evaluation. The porosity – permeability relation shows the general trend of increasing permeability with increasing porosity. The large scatter in the relevant cross plot, especially for Abu Roash Formation, shows that a permeability prediction from porosity only is not significant. The correlations of magnetic susceptibility are great with grain density and specific internal surface  $S_{por}$  for all samples due to iron oxide filling the sample pore spaces.

The Susceptibility - Permeability cross plot for samples of both Bahariya and Abu Roash Formation shows increasing permeability with a decrease in magnetic susceptibility. The Porosity - Formation resistivity factor shows a good possibility to calculate the formation factor from porosity data. The well-known Archie's law between formation resistivity factor and porosity is confirmed by our data set and the resulting constant factor  $a = 3.96$  and cementation factors  $m = 2.05$  for the Bahariya Formation and resulting in constant factor  $a = 3.75$  and cementation factors  $m = 1.83$  for Abu Roash Formation from general Archie equation.

The determination of the form factor from the Börner equation has been determined. The interface conductivity has been determined from the imaginary part of conductivity. The relationship between the imaginary conductivity and the surface conductivity has been experimentally derived from the linear relationship  $\sigma'' = l \times \sigma'_{surf}$ . Resulting  $l = 0.032$  for samples of the Bahariya Formation and gradient  $l = 0.038$  for the Abu Roash Formation. a similar relationship was found when the normalized chargeability determined the dependence of the IP response was used in place of the single-frequency imaginary conductivity. The determination of the form factor from the Börner equation is slightly lower than that of the resistivity ratio.

P-wave velocity decreases in general with increasing porosity in all studied samples. It was shown that the application of the Wyllie model equation fails to provide a reliable prediction of porosity for fluid-saturated samples from the compressional wave velocity data.

## Acknowledgement

My appreciation is to the Egyptian Petroleum Authority to give us permission to work with the needed subsurface core sample data and publish the results. The authors would like to thank the Institute for Geophysics, Clausthal University of Technology, Germany, the Egyptian petroleum research institute, and Ain Shams University for supporting this study's findings.

## References

- Abuseda, H., Weller, A., Sattler, C.-D., Debschütz, W., (2016). Petrographical and petrophysical investigations of upper Cretaceous sandstones of the South West Sennan field, Western Desert, Egypt. *Arabian Journal of Geosciences* 9, 212.
- Alsuwaidi, M., Mohamed, A. A., Mansurbeg, H., Morad, S., Alsuwaidi, A., Al-Shalabi, E. W., Gomes, J., Al-Ramadan, K., Mohammed, I.Q., Farouk, S., (2021). Depositional and diagenetic controls on reservoir quality of microporous basinal lime mudstones (Aptian), United Arab Emirates. *Sedimentary Geology*, 420, 105925.
- Adler, P., Jacquin, C.G., Quiblier, J., (1990). Flow in simulated porous media. *International Journal of Multiphase Flow* 16, 691-712.
- Athmer W. (2006). Petrologische und petrophysikalische Charakterisierung der stark anisotropen Bahariya Formation (Ägypten). - In: Müller R (ed.): *Geoforschung 2006 - Beiträge aus Geologie, Paläontologie und Geophysik. – Clausthaler Geowissenschaften* 5:19–33.
- Archie, G.E., (1942). The electrical resistivity log is an aid in determining some reservoir characteristics. *Trans AIME*, Vol. 146, 45-62.
- Börner, F., Schopper, J., Weller, A., (1996). Evaluation of transport and storage properties in the soil and groundwater zone from induced polarization measurements. *Geophysical prospecting* 44, 583-601.
- Carman, P.C., (1937). Fluid flow through granular beds. *Trans. Inst. Chem. Eng.* 15, 150-166.
- Catuneanu, O., Khalifa, M.A., Wanas, H., (2006). Sequence stratigraphy of the lower Cenomanian bahariya formation, bahariya oasis, western desert, Egypt. *Sedimentary Geology* 190, 121-137.
- Dominik, W., (1985). *Stratigraphie und Sedimentologie (Geochemie, Schwermineralanalyse) der Oberkreide von Bahariya und ihre Korrelation zum Dakhla-Becken (Western Desert, Ägypten)*.
- El Gezeery, M., Mohsen, S., Farid, M., (1972). Sedimentary basins of Egypt and their petroleum prospects. *Proc 8th Arab Petrol Congr Algiers*, 1-15.
- El Sayed, A.M.A., (1981). *Geological and petrophysical studies for the Algyo-2 reservoir evaluation, Algyo oil and gas field, Hungary*. Ph. D. thesis, Hung. Acad. Sci., Budapest, 166.
- Farouk, S., Al-Zubi, H., Abdelkader, T., Ahmad, F., (2018). Facies associations and chemostratigraphy of the Lower Cretaceous Kurnub Group and their boundaries, King Talal Dam section, northwestern Jordan. *Environmental Geosciences*, v. 25, no. 1, pp. 1–23.
- Franks, G.D., (1982). Stratigraphical modeling of Upper Cretaceous sediments of Bahariya Oasis. *6th EGPC Exp. Seminar, Cairo*, 21 p.
- Glover, P., (2009). What is the cementation exponent? A new interpretation. *The Leading Edge* 28, 82-85.
- Halisch M, Weller A, Sattler C-D, Debschütz W, El-Sayed A.M.A., (2009). A complex core-log case study of an anisotropic sandstone, originating from Bahariya Formation, Abu Gharadig Basin, Egypt. *Petrophysics* 50:478–497
- Herron, M., M., (1987). Estimating of intrinsic permeability of elastic sediments from geochemical data *Trans., SPWLA*. P. 6
- Klinkenberg, L., (1941). The permeability of porous media to liquids and gases, *Drilling and production practice, OnePetro*.
- Rink, M., and Schopper, J., (1974). Interface conductivity and its implications to electric logging, *SPWLA 15th Annual Logging Symposium, Society of Petrophysicists and Well-Log Analysts*.
- Selim, S.S., Wafdy, R., Abu Khadrah, A.M., (2021). Sedimentological analysis and reservoir quality of the early Cenomanian transgressive sandstones, northern Western Desert, Egypt. *Journal of Petroleum Science and Engineering*, 197, 107948.
- Scheidegger, A., (1974). *The physics of flow through porous media*. The University of Toronto, Toronto Press, 353p.
- Schön, J.H., (1996). *Handbook of Geophysical Exploration: Fundamentals and Principles of Petrophysics. Seismic Exploration. Physical Properties of Rocks*. Pergamon.
- Soliman, S., and Hassan, M., (1970). Petrology of the Middle Miocene rocks of Gebel El Rusas, Ranga and Abu Anz localities, Eastern Desert, Egypt. *7th Arab Petrol. Congr., Kuwait* 60, 1-40.
- Tiab, D., and Donaldson, E.C., (2015). *Petrophysics: theory and practice of measuring reservoir rock and fluid transport properties*. Gulf professional publishing.
- Timur, A., (1968). An investigation of permeability, porosity, and residual water saturation relationships, *SPWLA 9th annual logging symposium, Society of Petrophysicists and Well-Log Analysts*.
- Vinegar, H., and Waxman, M., (1984). Induced polarization of shaly sands: *Geophysics*, 49, 1267 – 1287, DOI: 10.1190/1.1441755.
- Waxman, M. H., and Smits, L. J. M. (1968). Electrical conductivities in oil-bearing shaly sands: *SPE Journal*, 243, 107 – 122, DOI: 10.2118/1863-A.
- Wyllie, M., and Gregory, A., (1953). Formation factors of unconsolidated porous media: Influence of particle shape and effect of cementation. *Journal of petroleum technology* 5, 103-110.
- Wyllie, M., Gregory, A., Gardner, G., (1958). An experimental investigation of factors affecting elastic wave velocities in porous media. *Geophysics* 23, 459-493.
- Wyllie, M., and Spangler, M., (1952). Application of electrical resistivity measurements to the problem of fluid flow in porous media. *AAPG Bulletin* 36, 359-403.
- Wyllie, M.R.J., Gregory, A.R., Gardner, L.W., (1956). Elastic wave velocities in heterogeneous and porous media. *Geophysics* 21, 41-70.